Experimental study of a R290 variable geometry ejector

Giorgio Besagni[1], Fabio Inzoli[1], Lorenzo Croci[2], Vittorio Brignoli[2], Jacek Smolka[3], Michal Palacz[3], Michal Haida[3], Jakub Bodys[3], Rafal Fingas[3], Andrzej J. Nowak[3], Bartlomiej Melka[3], Michal Stebel[3], Edyta Piechnik[3]

[1]Politecnico di Milano, Department of Energy, via Lambruschini 4a, 20156, Milano (Italy)
[2]Ricerca sul Sistema Energetico – RSE S.p.A., Power System Development Department, via Rubattino 54, 20134, Milano (Italy)
[3]Silesian University of Technology, Department of Thermal Technology, Konarskiego 22, 44-100, 20156, Gliwice (Poland)

giorgio.besagni@polimi.it

Abstract. Ejectors are classified as fluid-dynamics controlled devices where the "*component-scale*" performances are imposed by the local-scale fluid dynamic phenomena. For this reason, ejector performances (measured by the pressure-entrainment ratio coordinate of the critical point) are determined by the connection of operation conditions, working fluid and geometrical parameters. Given such a connection, variable geometry ejector represents a promising solution to increase the flexibility of ejector-based systems. The present study aims to extend knowledge on variable geometry systems, evaluating the local and global performances of the R290 ejector equipped with a spindle. The prototype ejector was installed at the R290 vapour compression test rig adapted and modified for the required experimental campaign. The test campaign considered global parameter measurements, such as the pressure and the temperature at inlets and outlet ports together with the mass flow rates at both inlet nozzles, and the local pressure drop measurements inside the ejector. In addition, the experimental data were gathered for different spindle positions starting from fully open position the spindle position limited by the mass flow rate inside the test rig with the step of 1.0 mm.

1. Introduction

Ejector is a device constituted by a primary nozzle, a suction chamber, a mixing chamber, and a diffuser, as displayed in Figure 1. An "*high energy*" primary flow accelerates and expands through the primary nozzle creating a low-pressure region nearby the nozzle exit; subsequently, the secondary flow is entrained into the mixing chamber because of the vacuum-effect and the shear action between the primary and secondary flows. The primary and the secondary flows mix within the mixing chamber and the resulting stream moves into a diffuser where the high velocity fluid is gradually decelerated and increased in pressure due to subsonic conditions.

The entrainment, the pressure recovery, and the mixing effects provided by the ejector, makes it suitable to be employed in ejector refrigeration systems (*ERSs*; Figure 2a presents the layout of a standard ejector refrigeration system, *SERS*) [1]. In general, *ERSs* are promising alternative compared with compressor-based technologies owing to their reliability, limited maintenance, low initial and operational costs, and no working fluid limitations [2]; also, the generator of an *ERS* might exploit

low-grade heat energy, making *ERSs* valuable in contributing towards reducing electricity consumption in the residential sector [3].

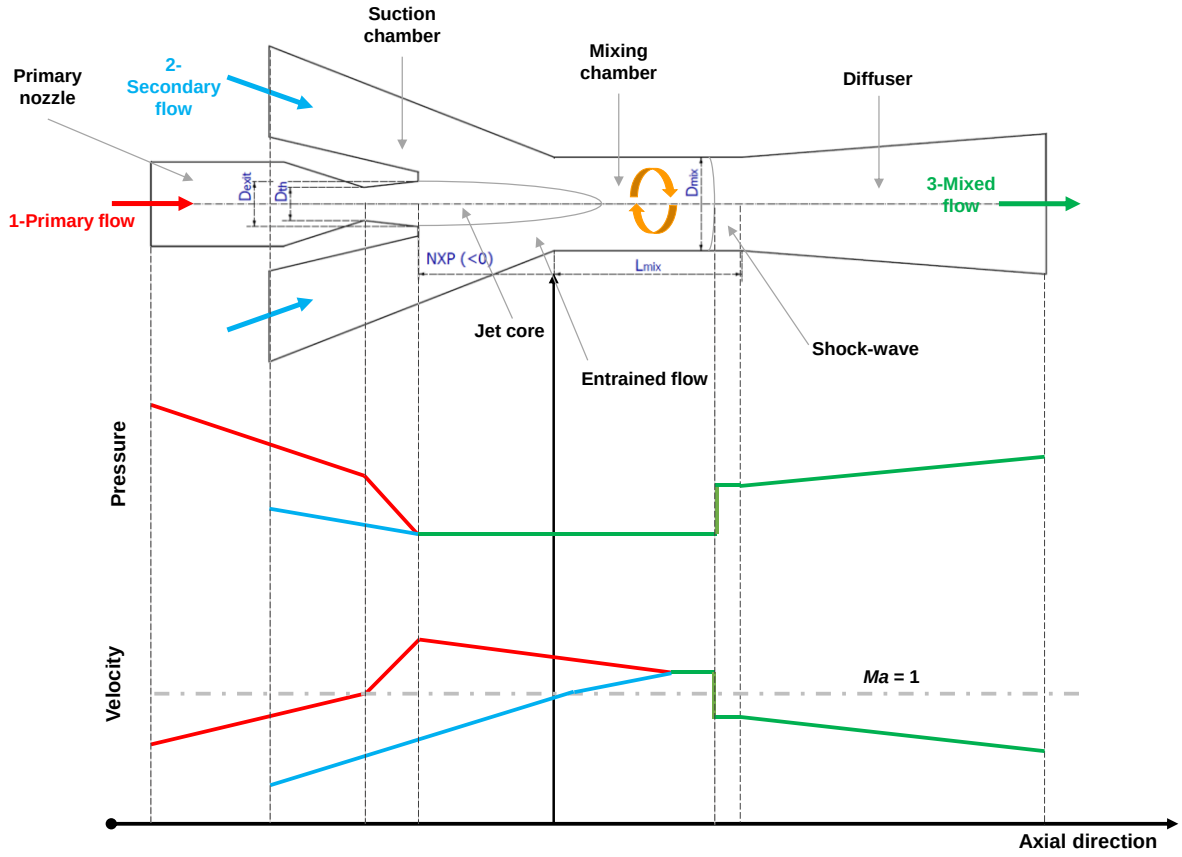

Figure 1. Ejector design and qualitative axial pressure and velocity trends

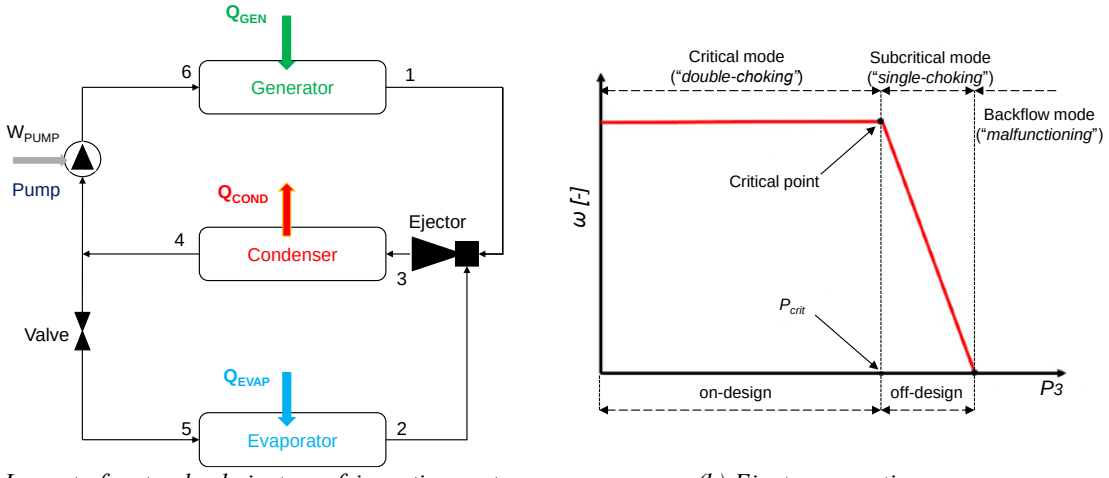

(a) Layout of a standard ejector refrigeration system *(b) Ejector operating curve*

Figure 2. Ejector component (a) and ejector refrigeration system (b)

Unfortunately, the large-scale deployment of *ERSs* is hindered owing to two main drawbacks: the low coefficient of performance (in the range of 0.1–0.7) and the relevant influence of ejector operation on the performance of the whole system. The latter can be easily explained by the fact that the ejector is a fluid-dynamics controlled device, where the fluid-dynamic interactions at the "*local-scale*" impact

on the performances at the "*component-scale*", namely the entrainment ratio ω (viz- the ratio between secondary and primary mass flow rates, Figure 2b). These multi-scale relationships can be easily explained considering that the ejector operation relies on two concurrent physical phenomena: (i) the low-pressure fluid entrainment process caused by the primary flow expansion and (ii) the compression effect, provided by the diffuser, which raises the secondary flow pressure from the evaporator to the condenser pressure. These two effects are contrasting, and an improvement of the former would deteriorate the latter. Hence, for a given nozzle area ratio, the ejector operating curve is imposed by the primary and secondary flow boundary conditions. On the other hand, Variable Geometry Ejectors (*VGE*) represent a promising solution to increase the flexibility and operation range of this component. In a *VGE*, the spindle acts on the nozzle area, and primary flow rate, and changes the ejector's response by adjusting its entrainment ratio accordingly with the requirements of the system (i.e., temperature set point, thermal load, …).

The present-day discussion regarding ejector technology is even more challenging owing to the current transition in refrigerants; given the European regulation aimed to limit the emission of fluorinated greenhouse gases, the existing market is expected to change sharply in the next years, and 3rd generation refrigerants (i.e., R134a) will be most likely replaced by natural (i.e., hydrocarbons) and 4th generation fluids (i.e., hydrofluoroolefins) [4]. Among new refrigerants, *R290* (propane) is promising owing to its favourable thermodynamic properties, which make it suitable for refrigeration applications in the medium-long views.

This paper aims at extending knowledge on *VGE* systems, evaluating the impact of a spindle-provided ejector operated with R290 on the performance of an *ERS*. In a previous study proposed by the authors, a *VGE* ejector operated with R290 has been designed and numerically studied [5]. Thus, the proposed study is an advancement compared with the present body of knowledge as it aims at experimentally evaluating the local and global performances of the R290 *VGE* ejector equipped with a spindle. The test campaign considered global parameter measurements, such as the pressure and the temperature at inlets and outlet ports together with the mass flow rates at both inlet nozzles, and the local pressure drop measurements inside the ejector.

2. Methods

2.1. Tested ejector

The tested ejector has been derived by Besagni and Cristiani [5] starting from Del Valle et al. [6]. It should be noted how, compared with Del Valle et al. [6], the mixing chamber diameter has been reduced to 4 mm to extend the on-design operating mode. The present ejector has been provided of a spindle (Figure 3) which can move axially within the primary nozzle.

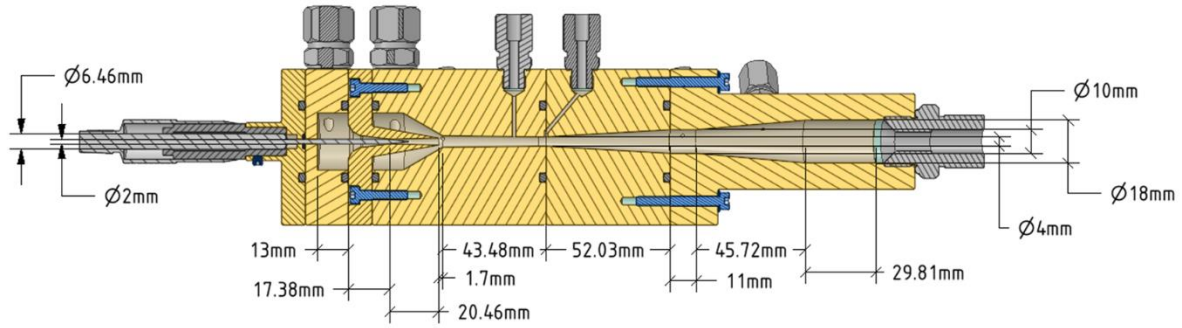

Figure 3. Ejector equipped with the spindle.

The neutral spindle position (*SP*) in which the tip of the spindle is placed right in the nozzle throat has been named as *SP*#0. Moving the spindle towards the nozzle exit, the nozzle throat area is reduced, and the area ratio is increased. The effects of the *SP* have been analysed in the range 0-8 mm, with a

discretization of 1 mm each position, whose code name will be referred as *SP#0.8*, depending on the *s*pindle position. It is worth noting that 8.0 mm corresponds to the unit minimum capacity (and *VGE*) for operation. The prototype device was manufactured, assembled, and tested with a high-pressure using nitrogen at 60 bar by TBT Technology in Gliwice, Poland. Figure 4 presents the manufactured ejector with the inlet/outlet ports, inner pressure drop ports, and the micrometer used to control the spindle position.

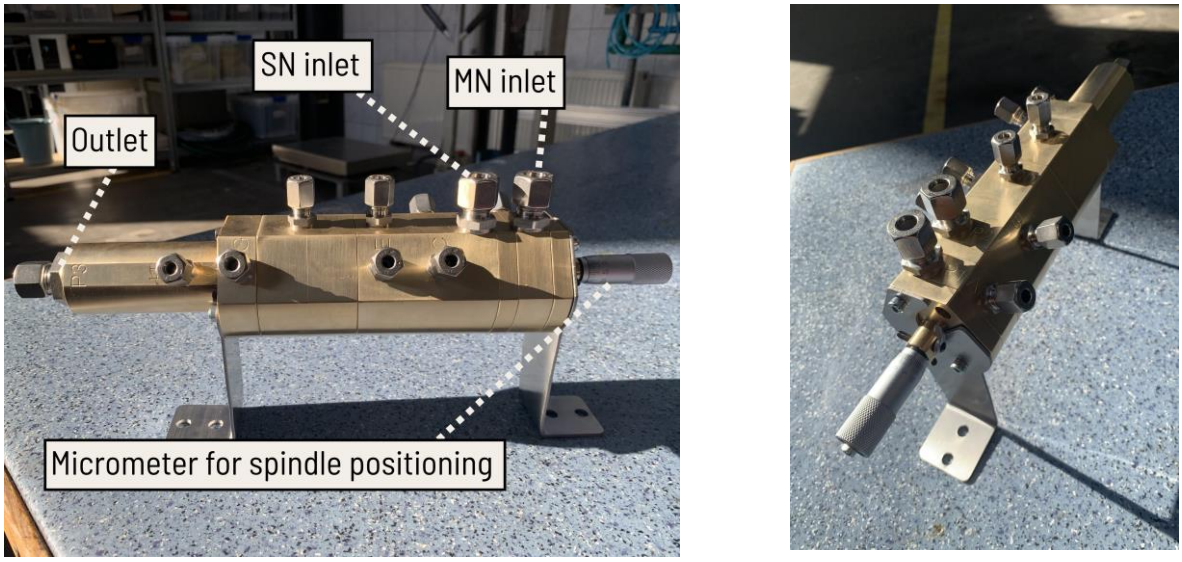

Figure 4. Manufactured R290 variable geometry ejector with spindle.

2.2. Test rig and instrumentation

Figure 5 presents the schematic diagram of the test rig used in this project and Table 1 lists the used instrumentation. All the pipes were covered with thermal polyethylene insulation that withstood the operating temperatures. The ejector inlet and outlet ports were connected with 10 mm copper pipes using Viton straight connectors. According to the goals of the present study, the detailed analysis of the performance of the *VGE* required precise instrumentation, as listed in Table 2. The temperature at the inlets of the ejector and the outlet was measured with calibrated T-type thermocouples. These sensors were attached to the copper walls of the inlet and outlet connectors. The thermal conductive paste was used to ensure proper contact of the sensors with the piping surface. Moreover, thermal insulation was installed at positions of thermocouples to minimize the influence of the ambient temperature on the thermocouple reading. Considering that one of the project aims was related to the definition of the pressure profile inside the ejector, the additional absolute pressure sensor was installed at the motive nozzle inlet. Furthermore, five differential pressure transducers were installed for measuring the pressure profile along the ejector. The mentioned differential pressure sensors marked as DP_1 to DP_5 are presented in Figure 6. It should be noted that the first of these sensors (DP_1) was used to measure the pressure drop inside the motive nozzle. Therefore, the measurement range of that pressure transducer was in the range of 0.0 to 25.0 bar, while the measurement range of DP_2 to DP_5 was in the range of 0.0 to 2.0 bar. The differential pressure sensors were connected with the prototype ejector in positions A-H presented in Figure 7. In the final setup of the system, positions B and G were closed. The high-pressure side for all the differential pressure transducers was defined with respect to the port located closer to the motive nozzle, e.g., in position A for A-C ports for DP_1. All the ports presented in Figure 8 are connected to differential pressure sensors as follows: position A-C - differential pressure sensor DP_1; position C-D - differential pressure sensor DP_2; position D-E - differential pressure sensor DP_3 :position E-F - differential pressure sensor DP_4; position F-H - differential pressure sensor DP_5.

Table 1. Description of the measurement instruments of the SUT R290 heat pump test rig.

Parameter	Sensor type	Model	Range and accuracy
Pressure	Gauge pressure, HP	Danfoss AKS32R	-1 ÷ 32 bar, 0,8% · x
	Gauge pressure, LP	Danfoss AKS32R	-1 ÷ 12 bar, 0,8%·*x*
Temperature	PT1000 RTD	Danfoss AKS11	- 40 ÷ 100 °C, ±0,3◦C
Mass flow rate	Coriollis type	E+H Cubemass C300	0 ÷ 90 kg/h, 0,1% *x*

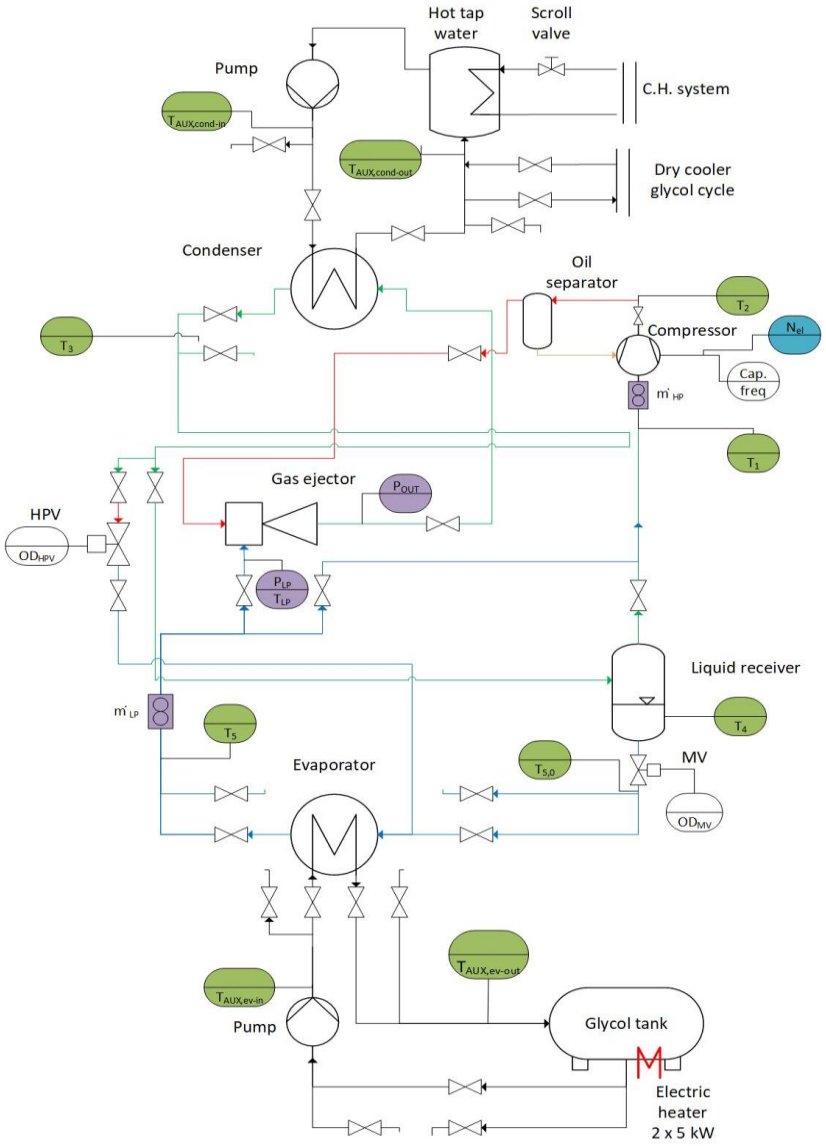

Figure 5. The PID scheme of the SUT R290 heat pump system.

Table 2. Description of the measurement instruments for the multi-scale study of the *VGE* ejector.

Parameter	Sensor type	Model	Range and accuracy
Pressure	Absolute pressure, MN	E+H Cerabar PMP51	0 ÷ 25 bar, 0,1% x
	Differential pressure, DP_1	E+H Deltabar PMD55	± 0 ÷ 25 bar, 0,1%·*x*
	Differential pressure, DP_{2-5}	E+H Deltabar PMD55	± 0 ÷ 2 bar, 0,1%·*x*
Temperature	T-type thermocouple	Termoaparatura TTP	-40 ÷ 350◦C, ±0,5◦C

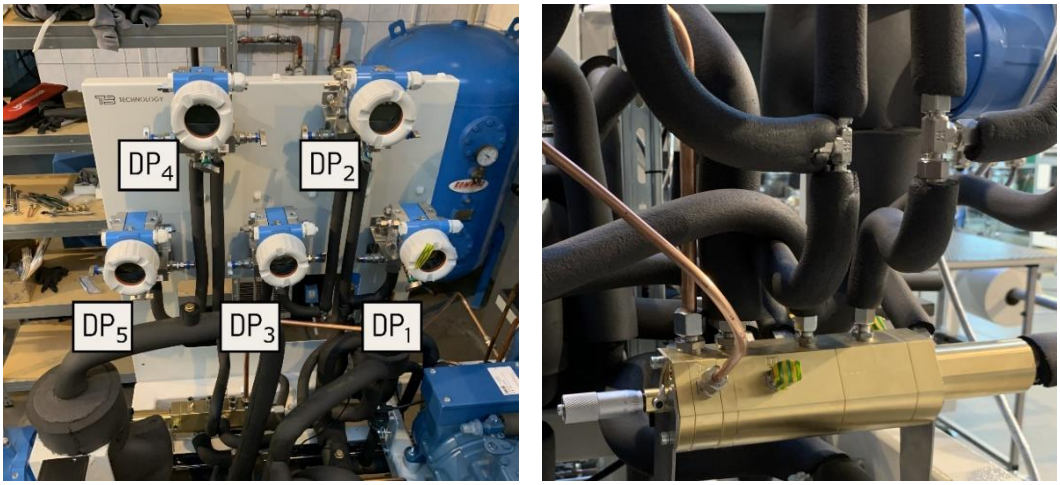

Figure 6. The board for the pressure sensors and the ejector.

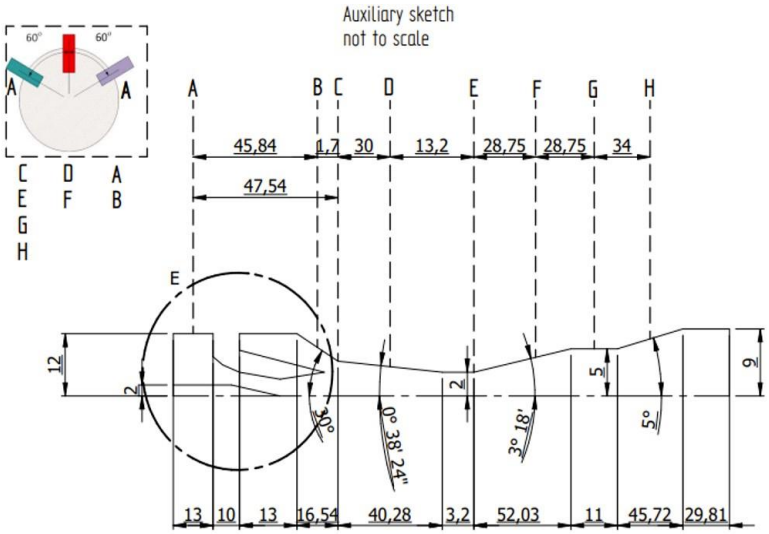

Figure 7. Cross-section of the VGE presenting the measurement ports positioning (A-H).

2.3. Data acquisition system

To ensure the required accuracy of the pressure and temperature measurements, the external data acquisition system was used. All the pressure and temperature sensors described in the previous sections were connected to the National Instruments (NI) cDAQ-9189. For the temperature measurements, a dedicated insulated thermocouple module with built-in cold junction temperature compensation was used (NI-9212). The analogue signals from the pressure transducers were captured with a current input module with an internal current loop (NI-9207). The linear functions defined for the sensors measurement range were used to convert the current signal to the pressure signal. To visualize and record all these signals, the NI LabView application was developed. The frequency of the data recording was set to 5 Hz for all of the investigated cases.

3. Results

The experimental results of these tests are presented in Table 3 and in Figure 8 (ω is the entrainment ratio and P_{lift} is the ratio between the outlet pressure and the secondary flow pressure). For each case,

the results were recorded during a period of 5 minutes of the heat pump operation after achieving steady-state conditions. The recorded time period was chosen based on the experimental investigation performed for R744 two-phase ejector. The data sampling frequency was 5 Hz for the motive nozzle pressure, pressure drops and temperatures. For the mass flow rates, the suction nozzle pressure and the outlet pressure, the sampling frequency was 0.2 Hz. All data were averaged, and type-A uncertainty was used to represent the deviation of the results.

Table 3. Experimental results for spindle positions *SP#1-SP#8*.

ID		P_1	T_1	$\dot{m}_1$	P_2	T_2	$\dot{m}_2$	P_3	T_3	$T_{3,}$	P_{lift}	ω
-		$[bar]$	$[°C]$	$[kg/h]$	$[bar]$	$[°C]$	$[kg/h]$	$[bar]$	$[°C]$	$[°C]$	$[bar]$	$[-]$
SP#1_OC1	Av.	17.08	77.61	34.50	4.67	24.57	4.30	5.30	53.35	52.26	0.63	0.12
	Dev.	0.09	2.28	0.00	0.05	0.63	0.00	0.05	2.99	2.98		
SP#1_OC2	Av.	17.75	88.83	35.04	4.99	27.32	4.28	5.60	66.84	65.62	0.61	0.12
	Dev.	0.07	1.35	0.18	0.05	0.29	0.09	0.01	1.45	1.43		
SP#1_OC3	Av.	18.56	96.30	36.01	5.36	28.43	4.30	5.95	74.20	72.88	0.59	0.12
	Dev.	0.08	1.23	0.06	0.05	0.20	0.00	0.05	1.25	1.23		
SP#2_OC1	Av.	18.40	84.55	36.18	5.09	25.63	4.30	5.69	58.93	57.66	0.60	0.12
	Dev.	0.01	2.67	0.27	0.03	0.70	0.00	0.02	3.52	3.57		
SP#2_OC2	Av.	18.77	95.30	35.70	5.24	28.50	4.30	5.86	72.67	71.38	0.61	0.12
	Dev.	0.16	1.27	0.30	0.06	0.21	0.00	0.06	1.30	1.28		
SP#3_OC1	Av.	18.43	90.82	35.50	5.30	27.50	4.60	5.90	67.52	66.27	0.60	0.13
	Dev.	0.03	1.41	0.00	0.00	0.38	0.00	0.00	1.80	1.79		
SP#4_OC1	Av.	19.16	101.14	33.55	5.13	32.17	4.10	5.77	75.66	74.24	0.63	0.12
	Dev.	3.12	1.23	0.15	0.05	8.13	0.00	0.05	1.70	1.70		
SP#5_OC1	Av.	15.46	95.45	33.36	5.11	31.45	4.08	5.74	72.46	70.98	0.63	0.12
	Dev.	0.06	0.63	1.38	0.21	0.29	0.13	0.23	0.98	0.98		
SP#5_OC2	Av.	17.20	87.59	25.88	3.90	26.27	3.30	4.47	62.63	61.35	0.57	0.13
	Dev.	0.03	0.95	0.56	0.00	0.39	0.00	0.05	1.42	1.40		
SP#6_OC1	Av.	18.37	87.21	22.87	3.50	24.54	3.20	4.00	59.45	58.26	0.50	0.14
	Dev.	0.07	1.02	0.18	0.00	0.31	0.00	0.00	1.23	1.23		
SP#7_OC1	Av.	17.77	76.80	17.06	3.20	23.51	1.86	3.50	47.41	46.85	0.30	0.11
	Dev.	0.06	0.50	0.14	0.00	0.29	0.89	0.00	0.94	0.91		
SP#8_OC1	Av.	19.17	76.73	12.50	2.76	26.11	0.00	2.95	47.32	46.21	0.19	0.00
	Dev.	0.04	0.15	1.24	0.20	0.02	0.00	0.20	0.09	0.07		

The motive nozzle pressure and temperature varied from approximately 15.5 bar to 19.2 bar and from approximately 76.7◦C to 101.1◦C, respectively. Furthermore, the suction nozzle pressure was from approximately 2.75 bar at SP#8_OC1 to 5.4 bar at SP#1_OC3 and the suction nozzle temperature differed from 24.5◦C at SP#1_OC3 to 32.2◦C at SP#4_OC1. Finally, the outlet pressure was reached in the range from approximately 3.0 bar at SP#8_OC1 to 6.0 bar at SP#1_OC3 and the outlet temperature was from approximately 47.0◦C at SP#8_OC1 to 76.0◦C at SP#4_OC1. The different operating conditions at both nozzles and the outlet together with the different spindle position caused the motive nozzle mass flow rate reduction. Hence, the motive nozzle mass flow rates presented in Table 4 decreased from approximately 36.0 kg/h at SP#1_OC3 to 12.5 kg/h at SP#8_OC1, which was approximately 27.0% of the highest mass flow rate obtained at SP#0_OC3. In addition, the pressure lift varied from 0.19 bar at SP#8_OC1 to 0.63 bar at SP#1_OC1 and ω was in the range from 0.0 at SP#8_OC1 to 0.14 at SP#6_OC1. Finally, the suction nozzle mass flow rate varied from 0.0 kg/h at SP#8_OC1 to 4.6 kg/h at SP#3_OC1 due to the reached ω at the specific pressure lift and motive nozzle conditions. Pressure drops DP_1-DP_5 shown in Figure 8 demonstrated that the highest pressure drop was reached for DP_1 from approximately 12.0 bar at SP#5_OC1 to 16.5 bar at SP#8_OC1. Then, the pressure increment was obtained for DP_2 from -0.25 bar at SP#8_OC1 to approximately -0.75 bar at SP#3_OC1. Furthermore, the lowest pressure increment was observed for highest mass flow rate reduction at SP#7 and SP#8. A minor pressure drop in the

range from 0.04 bar to approximately 0.2 bar was reached for DP_3 due to the mixing process inside the mixing section. The pressure increments at the first part of the diffuser from -0.08 bar at SP#8_OC1 to -0.36 bar at SP#1_OC3 was reached for DP_4. Finally, the negligible pressure increments of maximum -0.03 bar was obtained for DP_5.

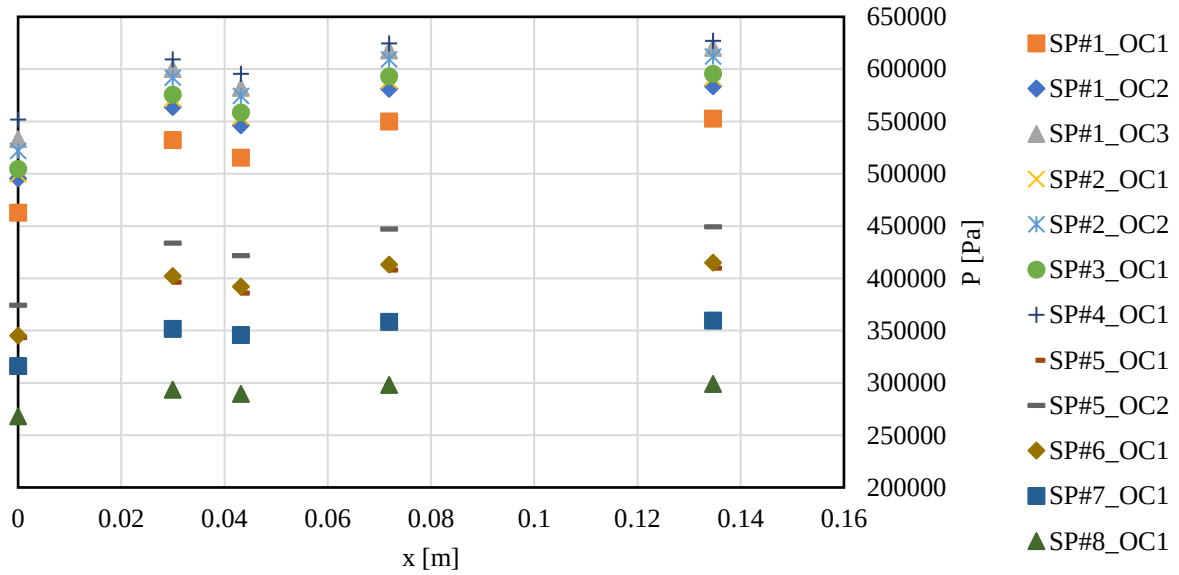

Figure 8. Local pressure drop measurements inside the ejector.

4. Conclusions

The aim of this work was to perform the experimental test campaign of the *VGE* prototype gas ejector using propane as the working fluid. The test campaign considered global parameter measurements and the local pressure drop measurements inside the ejector. The experimental data were gathered for different spindle positions starting from fully open position SP#0 to the spindle position limited by the mass flow rate inside the test rig with the step of 1.0 mm. It was found that the highest pressure drop was reached between the motive nozzle inlet and the half part of the pre-mixer due to the expansion process in the converging-diverging nozzle and the entrainment process in the pre-mixer. The pressure increment between the pre-mixer and the half-part of the converged mixing section was observed due to the sonic and expansion waves appeared near the inner ejector walls. In addition, the off-design conditions of the prototype ejector resulted in a low mass entrainment ratio below 0.2 for all the gathered experimental points. Future works will be devoted to extending this experimental study.

5. Acknowledgements

This work has been financed by the Research Fund for the Italian Electrical System in compliance with the Decree of Minister of Economic Development April 16, 2018.

6. References

[1] Aidoun Z, Ameur K, Falsafioon M and Badache M 2019 *Inventions* **4** 15
[2] Besagni G, Mereu R and Inzoli F 2016 *Renew. Sust. Energ. Rev.* **53** 373-407
[3] Knobloch F, Pollitt H, Chewpreecha U, Daioglou V and Mercure J F 2019 *Energ. Effic.* **12**(2) 521-550
[4] Cavallini A 2020 *J. Phys. Conf. Ser.* **1599** 012001
[5] Besagni G and Cristiani N 2021 *Appl. Therm. Eng.* **188** 116612
[6] Del Valle J G, Jabardo J S, Ruiz F C and Alonso J S J 2014. *Int. J. Refrig.* **46** 105-113